

## Salt Dependence of an $\alpha$ -Helical Peptide Folding Energy Landscapes<sup>†</sup>

Kan Xiong,<sup>‡</sup> Eliana K. Ascitutto,<sup>§</sup> Jeffry D. Madura,<sup>§</sup> and Sanford A. Asher<sup>\*,‡</sup>

<sup>‡</sup>Department of Chemistry, University of Pittsburgh, Pittsburgh, Pennsylvania 15260, and <sup>§</sup>Department of Chemistry and Biochemistry, Center for Computational Sciences, Duquesne University, Pittsburgh, Pennsylvania 15282

Received August 21, 2009; Revised Manuscript Received October 6, 2009

**ABSTRACT:** We used CD, UV resonance Raman spectroscopy, and molecular dynamics simulation to examine the impact of salts on the conformational equilibria and the Ramachandran  $\Psi$  angle (un)folding Gibbs free energy landscape coordinate of a mainly polyalanine  $\alpha$ -helical peptide, AP of sequence AAAAA-(AAARA)<sub>3</sub>A. NaClO<sub>4</sub> stabilizes  $\alpha$ -helical-like conformations more than does NaCl, which stabilizes more than Na<sub>2</sub>SO<sub>4</sub> at identical ionic strengths. This  $\alpha$ -helix stabilization ordering is the reverse of the Hofmeister series of anions in their ability to disorder water hydrogen bonding. Much of the NaClO<sub>4</sub>  $\alpha$ -helix stabilization results from ClO<sub>4</sub><sup>−</sup> association with the AP terminal  $-\text{NH}_3^+$  groups and Arg side chains. ClO<sub>4</sub><sup>−</sup> stabilizes 3<sub>10</sub>-helix conformations but destabilizes turn conformations. The decreased Cl<sup>−</sup> and SO<sub>4</sub><sup>2−</sup> AP  $\alpha$ -helix stabilization probably results from a decreased association with the Arg and terminal  $-\text{NH}_3^+$  groups. Cl<sup>−</sup> is expected to have a smaller binding affinity and thus stabilizes  $\alpha$ -helical conformations intermediately between NaClO<sub>4</sub> and Na<sub>2</sub>SO<sub>4</sub>. Electrostatic screening stabilizes  $\pi$ -bulge conformations.

The mechanism(s) whereby peptides and proteins fold into their native states are poorly understood (1–6). The well-known Levinthal paradox (7) clearly demonstrates that proteins do not fold through a random search of their conformational space since this would take longer than the age of our universe. Recent energy landscape models (1, 3, 8, 9) propose that funnel-shaped folding energy landscapes occur, where the native state is accessed via a strategically sloped energy landscape that funnels unfolded conformations toward the native folded state (3, 10, 11).

In the work here we use CD, UV resonance Raman spectroscopy (UVRR), and molecular dynamics simulation to examine the Gibbs free energy landscape along the  $\Psi$  Ramachandran angle folding coordinate of a mainly polyalanine peptide, AP of sequence AAAAA-(AAARA)<sub>3</sub>A, in pure water and in the presence of NaClO<sub>4</sub>, NaCl, and Na<sub>2</sub>SO<sub>4</sub>. AP-like peptides have been the subject of extensive experimental (12–30) and theoretical (31–42) studies which have probed the mechanism(s) of  $\alpha$ -helix folding and unfolding. The AP peptide is  $\sim 50\%$   $\alpha$ -helical-like at 0 °C and melts to PPII-like conformations at higher temperatures (43–47). We previously found that AP (un)folding is not a simple two-state process because it involves other secondary structure conformations such as  $\pi$ -bulge and 3<sub>10</sub>-helix and turn structures (22, 31, 32, 41, 42, 48, 49). We examined the dependence of the AP conformational equilibrium and melting on the presence of different salts and find that ion binding and electrostatic screening significantly modulate the Gibbs free energy landscape and stabilize  $\alpha$ -helix conformations. We also find that the ordering of salt stabilization of the  $\alpha$ -helical content can be explained by Collins et al. “law of matching water affinities” (50–52).

### EXPERIMENTAL PROCEDURES

The 21-residue peptide AP of sequence AAAAA-(AAARA)<sub>3</sub>A was purchased from AnaSpec Inc. (>95% purity). Anhydrous

NaCl, NaClO<sub>4</sub>, and Na<sub>2</sub>SO<sub>4</sub> were purchased from J. T. Baker (>99% purity). All AP samples were prepared at 1.0 mg/mL concentrations at pH 7.

The CD spectra were measured by using a Jasco-715 spectropolarimeter, using a 200  $\mu\text{m}$  path length cuvette. We coadded ten individual spectra.

The UVRR spectrometer was described in detail by Bykov et al. (53). Briefly, 204 nm UV light was obtained by generating the fifth anti-Stokes Raman harmonic of the third harmonic of a Nd:YAG laser (Coherent, Infinity). We used a spectral accumulation time of 5 min for each measurement and coadded four accumulations.

**Molecular Dynamics Simulation.** We performed replica exchange molecular dynamics (REMD) studies of AP immersed in pure water and in a 0.2 M NaClO<sub>4</sub> aqueous solution. The temperatures studied range from 270 to 505 K. The simulation details are given in the Supporting Information. To investigate the mechanisms which govern helix stabilization, we used Chimera (54) to calculate the average ion occupancy surrounding the AP peptide.

### RESULTS

**CD Results.** Figure 1 shows the temperature dependence of the CD spectra of AP in pure water. The lower temperature CD spectra show two troughs at 222 and 206 nm that are characteristic of  $\alpha$ -helix conformations (55). As the temperature increases, the ellipticity at 222 nm,  $\Theta_{222}$ , becomes less negative, indicating  $\alpha$ -helix melting. The isosbestic point at 202 nm indicates that this melting appears spectroscopically as a “two-state” process. Previous work by our group demonstrated that the AP  $\alpha$ -helix conformation melts to a dominantly PII-like conformation (56).

Addition of NaClO<sub>4</sub> (Figure 2a) increases the AP  $\alpha$ -helical content at all temperatures, as evident from the more negative values of  $\Theta_{222}$ ; however, the CD changes are relatively small between 1 and 2 M NaClO<sub>4</sub> concentrations. As discussed below,  $T_m$  also increases as the NaClO<sub>4</sub> concentration increases.

<sup>†</sup>This work was supported by NIH Grant GM8RO1EB002053.

<sup>\*</sup>To whom correspondence should be addressed. Phone: (412) 624-8570. Fax: (412) 624-0588. E-mail: asher@pitt.edu.

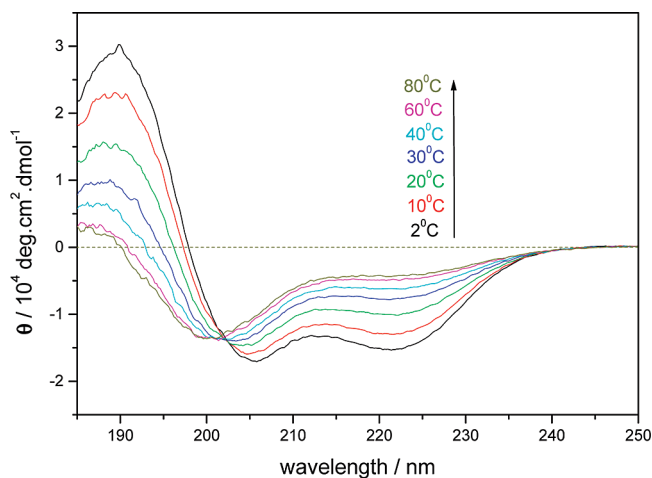


FIGURE 1: Temperature dependence of the CD spectra of AP in pure water at pH 7.

Table 1: Thermodynamic Parameters Calculated from CD Data

solution	$\Delta H/\text{kJ}\cdot\text{mol}^{-1}$	$\Delta S/\text{J}\cdot\text{mol}^{-1}\cdot\text{K}^{-1}$	$T_m/\text{K}^a$	$R^2$
pure water	$-33.4 \pm 1.4$	$-121 \pm 5$	276	0.995
0.2 M NaCl	$-36.4 \pm 1.1$	$-128 \pm 4$	284	0.998
1.0 M NaCl	$-41.8 \pm 1.4$	$-144 \pm 5$	290	0.998
2.0 M NaCl	$-42.1 \pm 1.0$	$-144 \pm 3$	292	0.999
0.2 M NaClO <sub>4</sub>	$-39.7 \pm 1.5$	$-140 \pm 5$	284	0.997
1.0 M NaClO <sub>4</sub>	$-35.5 \pm 0.5$	$-122 \pm 2$	291	0.999
2.0 M NaClO <sub>4</sub>	$-30.4 \pm 0.5$	$-104 \pm 2$	292	0.999
0.0667 M Na <sub>2</sub> SO <sub>4</sub>	$-33.5 \pm 0.5$	$-119 \pm 2$	281	0.999
0.333 M Na <sub>2</sub> SO <sub>4</sub>	$-33.7 \pm 0.6$	$-117 \pm 2$	288	0.999
0.667 M Na <sub>2</sub> SO <sub>4</sub>	$-32.4 \pm 1.5$	$-113 \pm 5$	287	0.997

<sup>a</sup>We did not calculate the  $T_m$  standard error because it is likely that its error is not dominated by random processes but instead is dominated by bias due to the ignored temperature dependencies of  $\Delta H$  and  $\Delta S$ .

Panels b and c of Figure 2 show similar AP melting curves for NaCl and Na<sub>2</sub>SO<sub>4</sub>. Again, the  $\alpha$ -helix fractions increase as evident from the more negative  $\Theta_{222}$  values as the salt concentrations increase. Again, little increase occurs between 1 and 2 M salt concentrations.

To quantitatively model  $\alpha$ -helix melting, we calculated the  $\alpha$ -helical conformational fraction,  $f_\alpha$ , using a two-state model (eq 1) by utilizing the reported  $\Theta_{222}$  values for the pure  $\alpha$ -helix ( $[\theta]_\alpha = -26000 \text{ deg}\cdot\text{cm}^2\cdot\text{dmol}^{-1}$ ) and the “pure melted” conformations ( $[\theta]_r = -3500 \text{ deg}\cdot\text{cm}^2\cdot\text{dmol}^{-1}$ ) (57).

$$f_\alpha = \frac{[\theta] - [\theta_r]}{[\theta_\alpha] - [\theta_r]} \quad (1)$$

As shown below, the structure is actually more complex than a two-state transition, but significant useful thermodynamics information associated with the resulting quasi-two-state transition can be extracted from the CD data.

We also calculated the melting thermodynamic parameters by fitting the calculated equilibrium  $\alpha$ -helix fraction,  $f_\alpha$  to

$$\ln K = \ln \frac{f_\alpha}{1 - f_\alpha} = \frac{-\Delta H}{R} \left( \frac{1}{T} \right) + \frac{\Delta S}{R} \quad (2)$$

The fits to eq 2 versus  $T^{-1}$  are highly linear with  $R^2$  values of  $>0.995$ . Table 1 lists the calculated values for  $\Delta H$ ,  $\Delta S$ , and the resulting estimated  $T_m$  values. Figure 3 shows that  $T_m$  increases for all salts as their concentrations increase (except at the highest

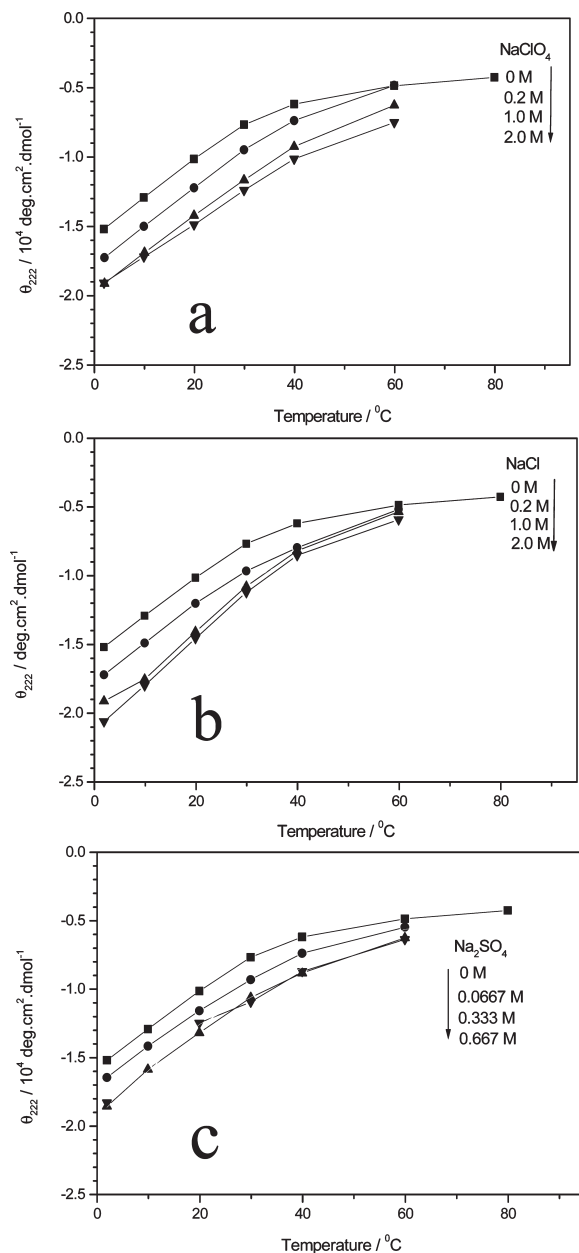


FIGURE 2:  $\Theta_{222}$  melting curve of AP (a) in NaClO<sub>4</sub> at different ionic strengths, (■) pure water, (●) 0.2 M NaClO<sub>4</sub>, (■) 1.0 M NaClO<sub>4</sub>, and (▼) 2.0 M NaClO<sub>4</sub>, (b) in NaCl at different ionic strengths, (■) pure water, (●) 0.2 M NaCl, (■) 1.0 M NaCl, and (▼) 2.0 M NaCl, and (c) in Na<sub>2</sub>SO<sub>4</sub> at various ionic strengths, (■) pure water, (●) 0.0667 M Na<sub>2</sub>SO<sub>4</sub>, (■) 0.333 M Na<sub>2</sub>SO<sub>4</sub>, and (▼) 0.667 M Na<sub>2</sub>SO<sub>4</sub>.

Na<sub>2</sub>SO<sub>4</sub> concentration). NaClO<sub>4</sub> and NaCl stabilize  $\alpha$ -helices more than does Na<sub>2</sub>SO<sub>4</sub>.  $T_m$  increases as the Na<sub>2</sub>SO<sub>4</sub> concentration increases to 0.333 M (ionic strength of 1.0 M) but then begins to decrease at a concentration of  $\sim 0.667$  M (ionic strength of 2.0 M).

$\Delta H$  becomes more negative as the NaClO<sub>4</sub> concentration increases to 0.2 M but then becomes less negative at higher NaClO<sub>4</sub> concentrations. A similar trend occurs for  $\Delta S$ . Thus, the  $\alpha$ -helix becomes more (less) favored enthalpically (entropically) as the salt concentration increases.  $\Delta G$ , the difference between  $\Delta H$  and  $T\Delta S$ , for  $\alpha$ -helix formation becomes more negative as the NaClO<sub>4</sub> concentration increases.

In contrast,  $\Delta H$  and  $\Delta S$  both become more negative as the NaCl concentration increases to 1.0 M, but the values saturate upon concentration increases to 2.0 M.

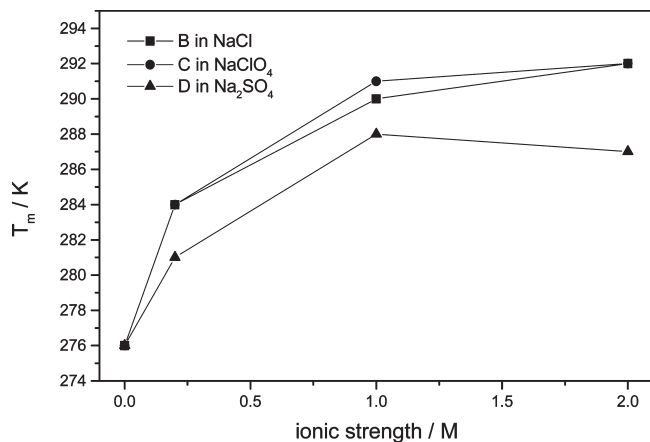
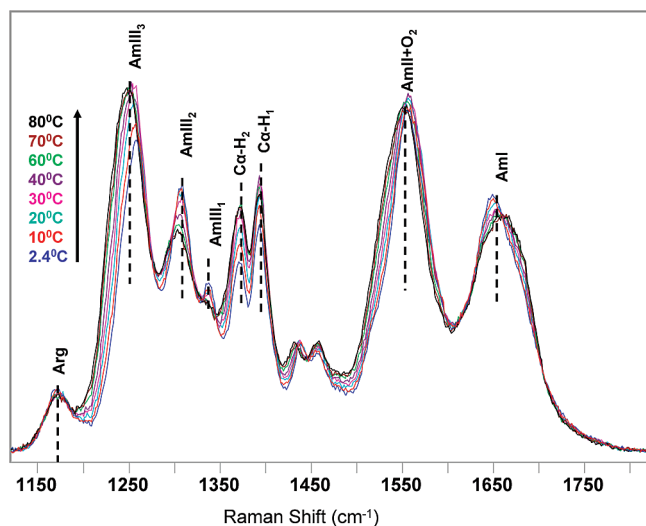
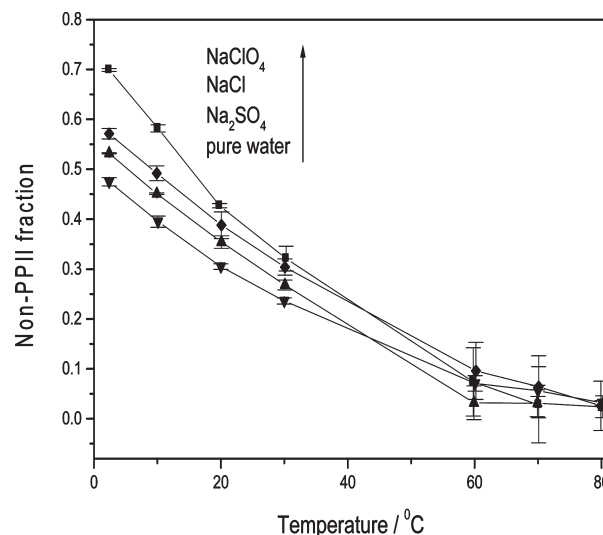
FIGURE 3: Calculated  $T_m$  of AP  $\alpha$ -helix melting in different salts.

FIGURE 4: Temperature dependence of 204 nm excited UVRR spectra of AP in pure water.

$\text{Na}_2\text{SO}_4$  also stabilizes the  $\alpha$ -helix giving rise to an increasingly negative  $\Delta G$ . However,  $\Delta H$  and  $\Delta S$  only show a modest dependence on the  $\text{Na}_2\text{SO}_4$  concentration. They both change together to make  $\Delta G$  increasingly negative as evident from the Figure 2c melting data for the lower concentrations.

**UV Resonance Raman Measurements.** Figure 4 shows the temperature dependence of the AP 204 nm UVRR spectra. The AmI band ( $\sim 1660\text{ cm}^{-1}$ ) results from a mainly C=O stretching vibration. The AmII band ( $\sim 1550\text{ cm}^{-1}$ ) derives from out-of-phase motion of C–N stretching and N–H bending. The  $\text{C}_\alpha$ –H doublet ( $\sim 1372$  and  $\sim 1393\text{ cm}^{-1}$ ) derives from a  $\text{C}_\alpha$ –H bending vibration which is resonance enhanced because of coupling of  $\text{C}_\alpha$ –H bending to N–H bending. The intensities of the  $\text{C}_\alpha$ –H bending bands increase as the concentration of nonhelical conformations increases (58). The AmIII bands arise from vibrations which involve in-phase contributions of C–N stretching and N–H bending. The AmIII region contains three subbands: the AmIII<sub>1</sub> band ( $\sim 1336\text{ cm}^{-1}$ ), the AmIII<sub>2</sub> band ( $\sim 1306\text{ cm}^{-1}$ ), and the AmIII<sub>3</sub> band ( $\sim 1250\text{ cm}^{-1}$ ).

The AmIII<sub>3</sub> band is the most conformationally sensitive because it involves  $\Psi$ -angle-dependent coupling between N–H bending and the  $\text{C}_\alpha$ –H bending motions (59). For example, the AmIII<sub>3</sub> band of the  $\alpha$ -helix appears at  $1258\text{ cm}^{-1}$  and contains little  $\text{C}_\alpha$ –H bending. However, it shifts to  $1247\text{ cm}^{-1}$  in the PPII

FIGURE 5: Non-PPII (primarily  $\alpha$ - +  $3_{10}$ - +  $\pi$ -helix) fractions of AP in different salt solutions: (■) in 0.2 M  $\text{NaClO}_4$ ; (◆) in 0.2 M  $\text{NaCl}$ ; (●) in 0.0667 M  $\text{Na}_2\text{SO}_4$ ; (▼) in pure water.

conformation (60) and contains significant  $\text{C}_\alpha$ –H bending. The  $\alpha$ -helix AmIII<sub>3</sub> band cross section is roughly half that of the PPII-like conformation because of the  $\alpha$ -helix conformation electronic transition hypochromism (61). As the temperature increases, the intensities of the  $\text{C}_\alpha$ –H bands increase, indicating  $\alpha$ -helix melting. Also, the AmIII<sub>3</sub> band frequency shifts from  $\sim 1258\text{ cm}^{-1}$  at 2 °C to  $\sim 1247\text{ cm}^{-1}$  at 80 °C.

The UVRR of AP in 0.2 M  $\text{NaCl}$ , 0.2 M  $\text{NaClO}_4$ , and 0.0667 M  $\text{Na}_2\text{SO}_4$  solutions all indicate  $\alpha$ -helix melting as the temperature increases (spectra not shown). The spectra of samples without  $\text{ClO}_4^-$  or  $\text{SO}_4^{2-}$  were normalized to the AmI band integrated intensity, which shows little variation upon peptide conformational changes (62).

To calculate the  $\alpha$ -helical fractions, we calculated the temperature-dependent basis spectra of the PPII-like conformation by using the method of Lednev et al. (57). We then digitally smoothed and then subtracted the appropriate amount of the PPII-like conformation basis spectra from the measured and smoothed UVRR of AP.

The relative amount of the PPII conformation subtracted is the maximum amount of the PPII basis spectrum which minimized the  $\text{C}_\alpha$ –H region intensity, with the constraint that no negative features occur in the difference spectrum. The basis spectral intensities subtracted are directly proportional to the concentration of the PPII conformation at each temperature (57). The resulting difference spectra should result only from non-PPII conformations and appear to be mainly  $\alpha$ -helix-like.

Figure 5, which shows the temperature dependence of the non-PPII fraction, indicates that  $\text{NaClO}_4$  is the most “helix”-stabilizing salt, followed by  $\text{NaCl}$ ,  $\text{Na}_2\text{SO}_4$ , and then pure water. These results agree with the CD results above and with the salt ordering previously observed by others (63).

Figure 6 shows the temperature dependence of the calculated non-PPII,  $\alpha$ -helix-like spectra of AP in  $\text{NaClO}_4$ ,  $\text{NaCl}$ , and  $\text{Na}_2\text{SO}_4$  and the difference spectra between the different salt solution spectra. At all temperatures we observe a triplet of bands which are the hallmark of  $\alpha$ -helix-like UVRR spectra. The 30 °C spectrum shows a change in the AmIII<sub>3</sub> band shape as earlier noted by Mikhonin and Asher (48). The 30 °C AmIII<sub>3</sub> band

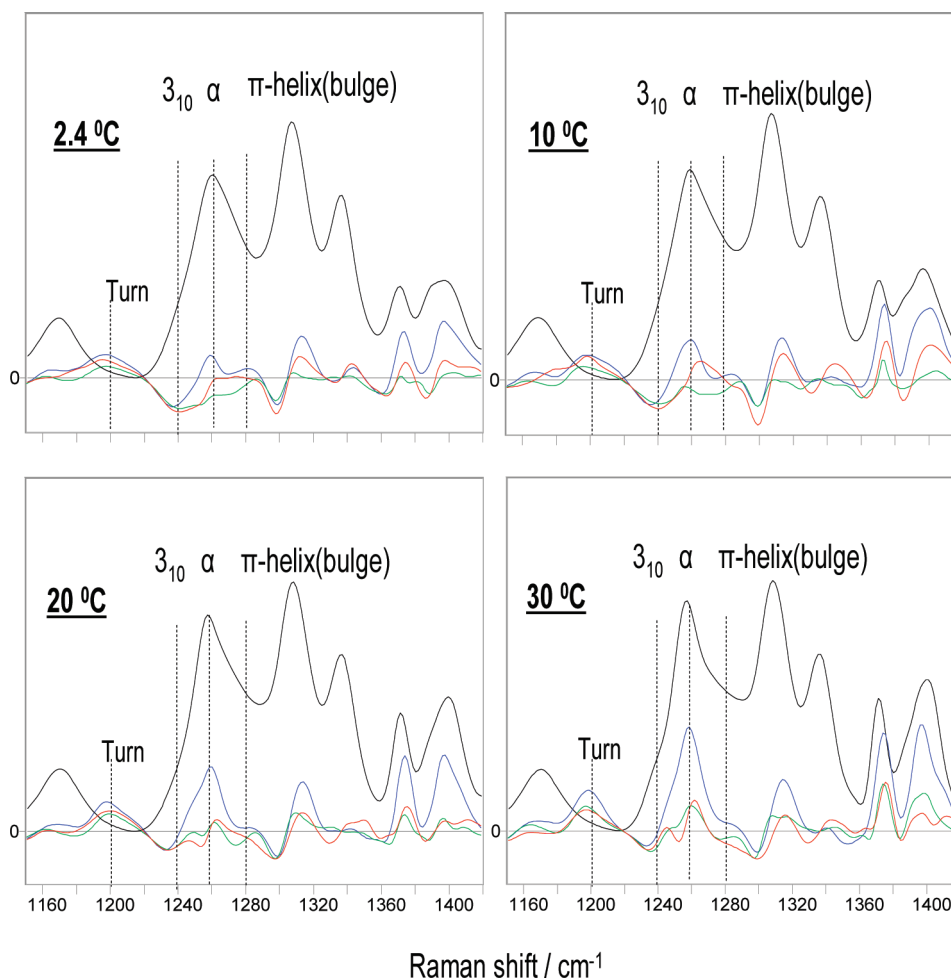


FIGURE 6: Temperature dependence of calculated  $\alpha$ -helix-like spectra in 0.2 M  $\text{NaClO}_4$  and difference spectra between different salt solutions: red, 0.2 M  $\text{NaCl}$  minus 0.2 M  $\text{NaClO}_4$ ; green, 0.0667 M  $\text{Na}_2\text{SO}_4$  minus 0.2 M  $\text{NaClO}_4$ ; blue, pure water minus 0.2 M  $\text{NaClO}_4$ . All displayed calculated  $\alpha$ -helix-like spectra were normalized to the intensity of the  $\text{AmIII}_1$  band of the 2.4 °C  $\alpha$ -helix-like spectrum in  $\text{NaClO}_4$ . The difference spectra between salts were calculated from these normalized spectra.

slightly narrows, while the maximum becomes more sharply peaked. This band shape change, which appeared as a more simple band narrowing in our previous poorer S/N spectra, was ascribed to a decrease in the concentrations of  $3_{10}$ -helix and  $\pi$ -bulge conformations relative to the  $\alpha$ -helix concentration as the temperature increases.

The most prominent difference between the different salt spectra is that a  $\sim 1200\text{ cm}^{-1}$  band that occurs in pure water, in  $\text{NaCl}$ , and in  $\text{Na}_2\text{SO}_4$  disappears in  $\text{NaClO}_4$  as indicated by the  $\sim 1200\text{ cm}^{-1}$  troughs in the difference spectra. A new band occurs at  $\sim 1240\text{ cm}^{-1}$  in  $\text{NaClO}_4$  solution, as evident by the trough in the difference spectra between the  $\text{NaClO}_4$  solution and the other salts and pure water (most clearly at temperatures below 20 °C). Previous work (48, 62) indicated that an  $\text{AmIII}_3$  band at  $\sim 1200\text{ cm}^{-1}$  derives from turn structures, while the  $\text{AmIII}_3$  band at  $\sim 1240\text{ cm}^{-1}$  derives from  $3_{10}$ -helix conformations. Therefore, we conclude that  $\text{NaClO}_4$  selectively stabilizes  $3_{10}$ -helix conformations which are replaced in pure water, in  $\text{NaCl}$ , and in  $\text{Na}_2\text{SO}_4$  by turn conformations.

We calculated the Gibbs free energy landscapes of AP along the  $\Psi$ -folding coordinate from the UVRR (Figures 7 and 8) by using the methodology of Mikhonin et al. (48, 53, 60, 64). We calculate the  $\Psi$  angle probability distribution from the  $\text{AmIII}_3$  band shape and utilize the Boltzmann relationship to calculate the Gibbs free energy landscape.

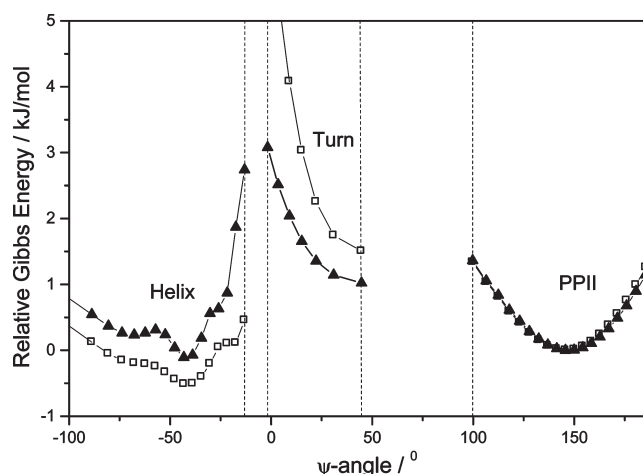


FIGURE 7: Calculated 2.4 °C Gibbs free energy landscape of AP in pure water ( $\blacktriangle$ ) and in 0.2 M  $\text{NaClO}_4$  ( $\square$ ). We use the PPII-like conformation as the reference state.

The calculated AP Gibbs free energy landscapes in pure water and in 0.2 M  $\text{NaClO}_4$  at 2.4 °C (Figure 7) show a broad  $\alpha$ -helix-like conformational region which includes  $\Psi$  angles corresponding to  $3_{10}$ -helices and  $\pi$ -bulges and the broad PPII region. The presence of 0.2 M  $\text{NaClO}_4$  selectively decreases the Gibbs free



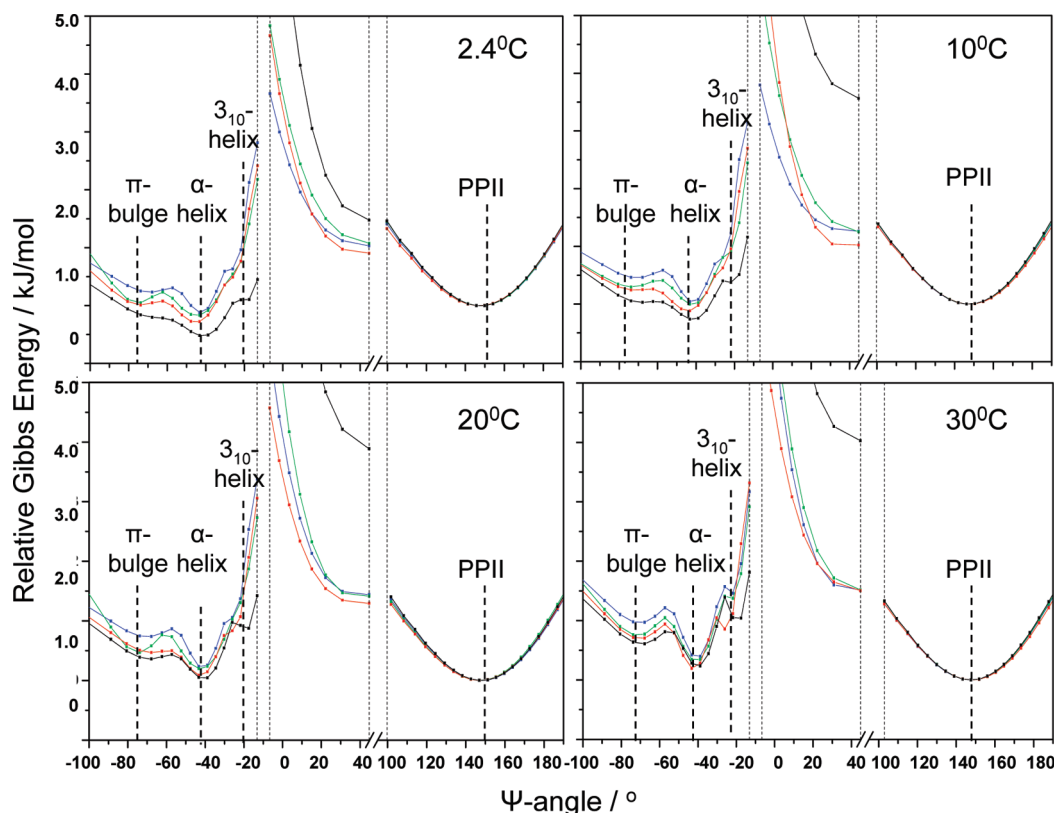


FIGURE 8: Calculated Gibbs free energy landscape of AP along the Ramachandran  $\Psi$  angle coordinate: in pure water (blue); in 0.0667 M  $\text{Na}_2\text{SO}_4$  (green); in 0.2 M  $\text{NaCl}$  (red); in 0.2 M  $\text{NaClO}_4$  (black). The PPII-like conformation is the reference state.

energies of the  $3_{10}$ -helix conformations but increases the free energy of the turn conformations. The  $\alpha$ -helix-like region, the turn region, and the PPII region are separated by high activation barriers due to steric clashes. These results are consistent with the calculated  $\Phi$  and  $\Psi$  dependence of the Gibbs free energies of peptide conformations (65). High activation energies are expected between  $\alpha$ -helix and turn conformations and PPII conformations. Our ability to monitor turn conformations is important for insight into the mechanisms of  $\alpha$ -helix melting since these turn conformations are likely to serve as intermediates along the reaction coordinates that link  $\alpha$ -helix-like to the melted PPII-like conformations (66, 67).

The energy landscape (Figure 8) is bumpy within the  $\alpha$ -helix-like basin. Within this basin the pure  $\alpha$ -helix conformation ( $\Psi \sim -45^\circ$ ) is always lowest in energy, followed by the  $\pi$ -bulge conformation ( $\Psi \sim -70^\circ$ ). The  $3_{10}$ -helix conformation ( $\Psi \sim -20^\circ$ ) lies at a slightly higher energy. Both the  $\pi$ -bulge and  $3_{10}$ -helix conformations appear to show activation barriers between their minima and that of the  $\alpha$ -helix conformation. The relative energy of the  $\pi$ -bulge conformation compared to the  $\alpha$ -helix conformation is highest in pure water. As the temperature increases, the  $\alpha$ -helix basin Gibbs free energy increases, indicating that the  $\alpha$ -helix is destabilized relative to the PPII conformation. We have drawn the energy landscape as a projection onto the  $\Psi$  angle coordinate. Traversing the energy landscape from one conformation to another could involve complex dynamics and involve significant dynamics involving  $\Phi$  angle excursions and excursions in other coordinates.

Figure 8 also shows the dependence of the conformational energies as a function of the salts dissolved in the AP solution at 0.2 M ionic strengths. For all temperatures, the lowest  $\alpha$ -helix Gibbs free energies occur in the presence of  $\text{NaClO}_4$ , followed by

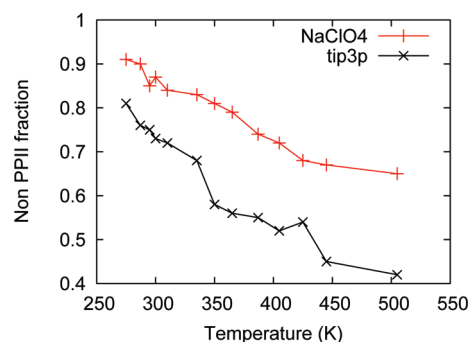


FIGURE 9: Molecular dynamics calculated AP non-PPII fraction in 0.2 M  $\text{NaClO}_4$  solution and in pure water by REMD simulations. The molecular dynamics predicted AP  $\alpha$ -helical conformation melting temperatures are higher than the experimental values because current force fields overstabilize the  $\alpha$ -helical conformation (68). Also, REMD simulations often predict much higher melting temperatures than standard MD simulations because the dynamical information is distorted by the REMD simulation temperature exchange process (69).

$\text{NaCl}$ ,  $\text{Na}_2\text{SO}_4$ , and pure water. The  $3_{10}$ -helix conformation is selectively stabilized by  $\text{NaClO}_4$ .

**Molecular Dynamics Simulation.** The  $\text{NaClO}_4$   $\alpha$ -helix stabilization was qualitatively reproduced by REMD simulations. Figure 9 shows the theoretically calculated AP non-PPII fraction as a function of temperature in 0.2 M  $\text{NaClO}_4$  solution and in pure water (all conformations with dihedral angles  $\Psi < +50^\circ$  are counted as non-PPII conformations). The AP  $\alpha$ -helical-like conformation (non-PPII conformations) concentrations in  $\text{NaClO}_4$  are greater than in pure water at all temperatures.

To investigate the mechanisms governing the helical stabilization, we studied the equilibrium  $\text{ClO}_4^-$  distribution around AP.

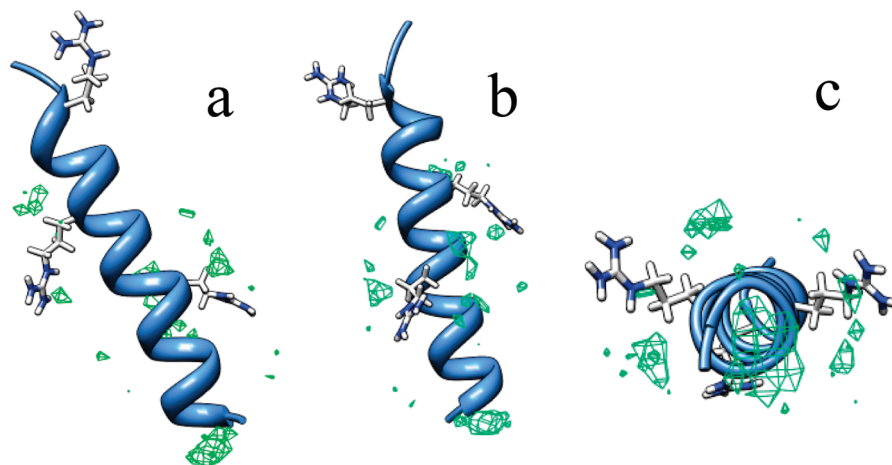


FIGURE 10:  $\text{ClO}_4^-$  occupancy around AP. The green contour shapes represent a higher than normal probability of finding  $\text{ClO}_4^-$  in a volume element near AP. (b) results from rotating (a)  $180^\circ$  about the helix axis; (c) looking down the helix axis from the N-terminus to the C-terminus.

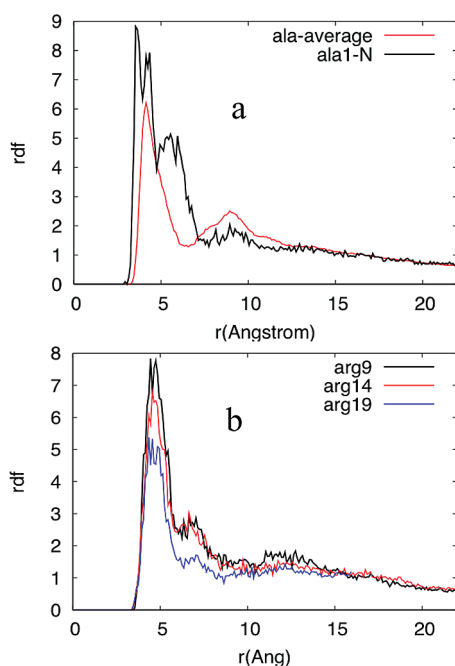


FIGURE 11: Average radial distribution functions of  $\text{ClO}_4^-$  with (a) the average Ala residue and the terminal  $-\text{NH}_3^+$  and (b) the different Args.  $r$  is the distance between the Cl in  $\text{ClO}_4^-$  and the  $\beta$  carbon of Ala or the nitrogen of the terminal  $-\text{NH}_3^+$  or the Arg  $\zeta$  carbon.

The average  $\text{ClO}_4^-$  concentrations around AP were calculated by using Chimera (54), where we calculated the average occupancy of  $\text{ClO}_4^-$  within a 3D grid over the trajectory frames. Figure 10 shows the concentration distribution where a green volume indicates a region of increased  $\text{ClO}_4^-$  occupancy.

The largest increased  $\text{ClO}_4^-$  occupancy occurs around the N-terminus. Panels a and b of Figure 10 also show increased  $\text{ClO}_4^-$  occupancies around Arg 9 and Arg 14, with no increased  $\text{ClO}_4^-$  occupancy around Arg 19, presumably due to the neutralization of Arg 19 charge by the carboxylate. Figure 10c shows that the  $\text{ClO}_4^-$  occupancy increases in the region between the Arg side chain and the peptide backbone.

Panels a and b of Figure 11, which show the radial distribution functions for  $\text{ClO}_4^-$ , for the average  $\beta$ -carbon of Ala, the terminal  $-\text{NH}_3^+$ , and the three different Arg  $\zeta$ -carbons, indicate that  $\text{ClO}_4^-$  is located on the average  $4.5 \text{ \AA}$  from the Ala  $\beta$  carbon and  $\sim 4 \text{ \AA}$  from the terminal  $-\text{NH}_3^+$  nitrogen, while it is on the

average  $\sim 5 \text{ \AA}$  from the Arg  $\zeta$  carbon. The distribution of  $\text{ClO}_4^-$  around the terminal  $-\text{NH}_3^+$  is highest, indicating that the largest association of  $\text{ClO}_4^-$  with AP occurs around the terminal  $-\text{NH}_3^+$ . Arg 9 has the highest affinity for  $\text{ClO}_4^-$ , followed by Arg 14 and then Arg 19.

$\text{ClO}_4^-$  binding to the terminal  $-\text{NH}_3^+$  and to Arg is expected from Collion's matching water affinity model (50–52) where ion pair formation occurs preferentially between oppositely charged ions of similar charge densities. In this model oppositely charged small ions of high charge density tend to preferentially form ion pairs. Large ions of low charge density also preferentially form ion pairs. Ion pairing between oppositely charged ions of high and low charge density is less favorable. Thus, for AP we expect that the weakly hydrated (with low charge density) N-terminal and Arg side chains (50–52) will most strongly bind to the weakly hydrated, low charge density  $\text{ClO}_4^-$  which will promote neutralization of the electrostatic interactions within AP which will significantly stabilize the  $\alpha$ -helix conformation.

## DISCUSSION

Both the CD and UVRR results show that salts stabilize  $\alpha$ -helical-like conformations of AP, with efficiencies:  $\text{NaClO}_4 > \text{NaCl} \sim \text{Na}_2\text{SO}_4$ . Numerous previous studies (71, 71) have proposed that these salts affect the protein/peptide stability through three main effects.

(1) The Hofmeister effect (72) phenomenon proposes that salts differentially “salt-in” or “salt-out” proteins/peptides by differentially interacting with water molecules, leaving less water available for protein/peptide hydration. The Hofmeister series orders ions in their decreasing ability to perturb water structure. For example,  $\text{SO}_4^{2-}$  precedes  $\text{Cl}^-$  in the Hofmeister series and thus will more efficiently “salt-out” proteins/peptides.  $\text{SO}_4^{2-}$  will preferentially dehydrate the AP backbone and should stabilize  $\alpha$ -helix-like conformations (14, 73–75).  $\text{ClO}_4^-$  follows  $\text{Cl}^-$  and will “salt-in” proteins/peptides by interacting weakly with water, which leaves more water available for protein/peptide hydration. This predicts that  $\text{ClO}_4^-$  should better stabilize melted, water-hydrogen-bonded PPII-like conformations.  $\text{Cl}^-$  should have an intermediate dehydration impact compared to  $\text{SO}_4^{2-}$  and  $\text{ClO}_4^-$ .

(2) Ionic screening decreases electrostatic interactions between protein and peptide charges (76). Higher ionic strengths increasingly screen electrostatic interactions between charges, as well as between charges and the helix dipole which can impact  $\alpha$ -helix

Table 2: Impact of Ions on AP  $\alpha$ -Helix Stability<sup>a</sup>

solution	ionic screening	Hofmeister effect	specific ion binding
pure water	0	0	0
NaCl	+	0	+
NaClO <sub>4</sub>	+	—	+
Na <sub>2</sub> SO <sub>4</sub>	+	+	0

<sup>a</sup>(+) helix stabilizing; (—) helix destabilizing; (0) no impact.

stability. For AP at pH 7, interactions between the  $\alpha$ -helix dipole and the N-terminal positive charge, as well as the anionic carboxylate C-terminal charge, destabilize the  $\alpha$ -helical conformation (77–79). In addition, electrostatic repulsions between the three Arg side chains should destabilize the  $\alpha$ -helix. Electrostatic screening by high ionic strength solutions will decrease these unfavorable interactions and will thus stabilize  $\alpha$ -helical-like conformations.

(3) Specific ion binding between solution ions and peptide and protein side chains can impact the  $\alpha$ -helix stability according to the Collins et al. (50–52) model of matching water affinities where ion pair formation is predicted on the basis of preferential formation between oppositely charged ions of similar charge densities. Small ions of high charge density (kosmotropes) tend to preferentially form ion pairs. In contrast, large ions of low charge density (chaotropes) form ion pairs between themselves. Hydrated ion pairing between kosmotropes and chaotropes is less favorable.

Thus, for AP we expect that the weakly hydrated N-terminal and Arg side chains (50–52) most strongly bind to the weakly hydrated chaotrope ClO<sub>4</sub><sup>−</sup>. The resulting charge neutralization will decrease electrostatic interactions within AP which should significantly stabilize the  $\alpha$ -helix conformation. Our molecular dynamics simulations directly observe association of ClO<sub>4</sub><sup>−</sup> with the terminal NH<sub>3</sub><sup>+</sup> group and the Arg. SO<sub>4</sub><sup>2−</sup> is expected to show the least ion pairing with NH<sub>3</sub><sup>+</sup> and Arg, while Cl<sup>−</sup> should show intermediate ion pairing. These ion pairing propensities predict that NaClO<sub>4</sub> should be the most helix stabilizing, followed by NaCl and then Na<sub>2</sub>SO<sub>4</sub>.

Table 2 summarizes the expected impact of ions on AP  $\alpha$ -helix stability from different effects. Our observations show that at identical ionic strengths  $\alpha$ -helical-like conformations are most stabilized by NaClO<sub>4</sub>, followed by NaCl, then Na<sub>2</sub>SO<sub>4</sub>, and then pure water. For NaClO<sub>4</sub> to exhibit the most stabilization, the positive impact from the specific ion binding effect must override the negative impact of the Hofmeister effect. The fact that NaCl stabilizes  $\alpha$ -helical-like conformations less than does NaClO<sub>4</sub> but more than Na<sub>2</sub>SO<sub>4</sub> suggests that the Hofmeister effect (water structure modification) has little impact.

The fact that  $\pi$ -helix (bulge) is disfavored in pure water but is stabilized in the presence of these three salts demonstrates that importance of electrostatic screening, where formation of the  $\pi$ -bulge must overcome repulsion between Arg side chains spaced at  $i, i + 5$  positions. In contrast, the Arg side chains are spaced further apart for the  $\alpha$ -helix and the <sub>310</sub>-helix. We are continuing to study why NaClO<sub>4</sub> stabilizes the <sub>310</sub>-helix but destabilizes the turn structure.

## CONCLUSION

We used CD and UV resonance Raman spectroscopy and molecular dynamics to study the solution conformation of a mainly polyalanine peptide containing Arg groups for solubility.

We calculated the Gibbs free energy landscape along the Ramachandran  $\Psi$  angle folding coordinate. We observe that at identical ionic strengths  $\alpha$ -helical-like conformations are stabilized most by NaClO<sub>4</sub> due to preferential ion binding of ClO<sub>4</sub><sup>−</sup> to the terminal NH<sub>3</sub><sup>+</sup> and Arg side chains. ClO<sub>4</sub><sup>−</sup> stabilizes <sub>310</sub>-helices but destabilizes turn conformations. Cl<sup>−</sup> has a smaller binding affinity and thus stabilizes  $\alpha$ -helical conformations intermediate between NaClO<sub>4</sub> and Na<sub>2</sub>SO<sub>4</sub>. Electrostatic screening stabilizes  $\pi$ -bulge conformations. We find that we can understand ion association to the peptide through the Collins “laws of matching water affinities model”.

## ACKNOWLEDGMENT

We thank Aleksandr V. Mikhonin, Zeeshan Ahmed, Bhavya Sharma, Lu Ma, and Zhenmin Hong for useful discussions.

## SUPPORTING INFORMATION AVAILABLE

Molecular dynamics simulation details. This material is available free of charge via the Internet at <http://pubs.acs.org>.

## REFERENCES

- Dill, K. A., Ozkan, S. B., Shell, M. S., and Weikl, T. R. (2008) The protein folding problem. *Annu. Rev. Biophys.* 37, 289–316.
- Ivarsson, Y., Travaglini-Allocatelli, C., Brunori, M., and Gianni, S. (2008) Mechanisms of protein folding. *Eur. Biophys. J. Biophys. Lett.* 37 (6), 721–728.
- Dobson, C. M., Sali, A., and Karplus, M. (1998) Protein folding: A perspective from theory and experiment. *Angew. Chem., Int. Ed.* 37 (7), 868–893.
- Baldwin, R. L., and Rose, G. D. (1999) Is protein folding hierarchic? II. Folding intermediates and transition states. *Trends Biochem. Sci.* 24 (2), 77–83.
- Baldwin, R. L., and Rose, G. D. (1999) Is protein folding hierarchic? I. Local structure and peptide folding. *Trends Biochem. Sci.* 24 (1), 26–33.
- Jahn, T. R., and Radford, S. E. (2005) The Yin and Yang of protein folding. *FEBS J.* 272 (23), 5962–5970.
- C. L. (1968) Are there pathways for protein folding? *J. Chem. Phys.* 65, 44–45.
- Dill, K. A., and Chan, H. S. (1997) From Levinthal to pathways to funnels. *Nat. Struct. Biol.* 4 (1), 10–19.
- Dill, K. A. (1999) Polymer principles and protein folding. *Protein Sci.* 8 (6), 1166–1180.
- Mello, C. C., and Barrick, D. (2004) An experimentally determined protein folding energy landscape. *Proc. Natl. Acad. Sci. U.S.A.* 101 (39), 14102–14107.
- Levy, Y., Jortner, J., and Becker, O. M. (2001) Solvent effects on the energy landscapes and folding kinetics of polyalanine. *Proc. Natl. Acad. Sci. U.S.A.* 98 (5), 2188–2193.
- Ihalainen, J., Bredenbeck, J., Pfister, R., Helbing, J., Chi, L., van Stokkum, I., Woolley, G., and Hamm, P. (2007) Folding and unfolding of a photoswitchable peptide from picoseconds to microseconds. *Proc. Natl. Acad. Sci. U.S.A.* 104 (13), 5383–5388.
- Balakrishnan, G., Hu, Y., Bender, G., Getahun, Z., DeGrado, W., and Spiro, T. (2007) Enthalpic and entropic stages in alpha-helical peptide unfolding, from laser T-Jump/UV Raman spectroscopy. *J. Am. Chem. Soc.* 129 (42), 12801–12808.
- Starzyk, A., Barber-Armstrong, W., Sridharan, M., and Decatur, S. (2005) Spectroscopic evidence for backbone desolvation of helical peptides by 2,2,2-trifluoroethanol: An isotope-edited FTIR study. *Biochemistry* 44 (1), 369–376.
- Wang, T., Zhu, Y., Getahun, Z., Du, D., Huang, C., DeGrado, W., and Gai, F. (2004) Length dependent helix-coil transition kinetics of nine alanine-based peptides. *J. Phys. Chem. B* 108 (39), 15301–15310.
- Huang, C., Getahun, Z., Zhu, Y., Klemke, J., DeGrado, W., and Gai, F. (2002) Helix formation via conformation diffusion search. *Proc. Natl. Acad. Sci. U.S.A.* 99 (5), 2788–2793.
- Huang, C., Klemke, J., Getahun, Z., DeGrado, W., and Gai, F. (2001) Temperature-dependent helix-coil transition of an alanine based peptide. *J. Am. Chem. Soc.* 123 (38), 9235–9238.
- Thompson, P., Munoz, V., Jas, G., Henry, E., Eaton, W., and Hofrichter, J. (2000) The helix-coil kinetics of a heteropeptide. *J. Phys. Chem. B* 104 (2), 378–389.



19. Yoder, G., Pancoska, P., and Keiderling, T. (1997) Characterization of alanine-rich peptides, Ac-(AAKAA)(n)-GY-NH<sub>2</sub> (n = 1–4), using vibrational circular dichroism and Fourier transform infrared. Conformational determination and thermal unfolding. *Biochemistry* 36 (49), 15123–15133.
20. Thompson, P., Eaton, W., and Hofrichter, J. (1997) Laser temperature jump study of the helix reversible arrow coil kinetics of an alanine peptide interpreted with a “kinetic zipper” model. *Biochemistry* 36 (30), 9200–9210.
21. Thompson, P., Eaton, A., and Hofrichter, J. (1997) Laser temperature jump studies of the helix-coil transition of an alanine-based peptide. *Biophys. J.* 72 (2), WP377–WP377.
22. Millhauser, G., Stenland, C., Hanson, P., Bolin, K., and vandeVen, F. (1997) Estimating the relative populations of 3(10)-helix and alpha-helix in Ala-rich peptides: A hydrogen exchange and high field NMR study. *J. Mol. Biol.* 267 (4), 963–974.
23. Williams, S., Causgrove, T., Gilmanshin, R., Fang, K., Callender, R., Woodruff, W., and Dyer, R. (1996) Fast events in protein folding: Helix melting and formation in a small peptide. *Biochemistry* 35 (3), 691–697.
24. Shalongo, W., Dugad, L., and Stellwagen, E. (1994) Distribution of helicity within the model peptide acetyl(AAQAA)<sub>3</sub>amide. *J. Am. Chem. Soc.* 116 (18), 8288–8293.
25. Fiori, W., Miick, S., and Millhauser, G. (1993) Increasing sequence length favors alpha-helix over 3(10)-helix in alanine-based peptides—evidence for a length-dependent structural transition. *Biochemistry* 32 (45), 11957–11962.
26. Scholtz, J. M., York, E. J., Stewart, J. M., and Baldwin, R. L. (1991) A neutral, water-soluble, alpha-helical peptide: The effect of ionic strength on helix-coil equilibrium. *J. Am. Chem. Soc.* 113, 5102–5104.
27. Marqusee, S., Robbins, V. H., and Baldwin, R. L. (1989) Unusually stable helix formation in short alanine-based peptides. *Proc. Natl. Acad. Sci. U.S.A.* 86, 5286–5290.
28. Ramajo, A. P., Petty, S. A., and Volk, M. (2006) Fast folding dynamics of alpha-helical peptides—Effect of solvent additives and pH. *Chem. Phys.* 323 (1), 11–20.
29. Silva, R. A. G. D., Kubelka, J., Bour, P., Decatur, S. M., and Keiderling, T. A. (2000) Site-specific conformational determination in thermal unfolding studies of helical peptides using vibrational circular dichroism with isotopic substitution. *Proc. Natl. Acad. Sci. U.S.A.* 97 (15), 8318–8323.
30. Long, H. W., and Tycko, R. (1998) Biopolymer conformational distributions from solid-state NMR: alpha-helix and 3(10)-helix contents of a helical peptide. *J. Am. Chem. Soc.* 120 (28), 7039–7048.
31. Wang, W., Lin, T., and Sun, Y. (2007) Examination of the folding of a short alanine-based helical peptide with salt bridges using molecular dynamics simulation. *J. Phys. Chem. B* 111 (13), 3508–3514.
32. Sorin, E., Rhee, Y., Shirts, M., and Pande, V. (2006) The solvation interface is a determining factor in peptide conformational preferences. *J. Mol. Biol.* 356 (1), 248–256.
33. Morozov, A., and Lin, S. (2006) Modeling of folding and unfolding mechanisms in alanine-based alpha-helical polypeptides. *J. Phys. Chem. B* 110 (41), 20555–20561.
34. Sorin, E., and Pande, V. (2005) Exploring the helix-coil transition via all-atom equilibrium ensemble simulations. *Biophys. J.* 88 (4), 2472–2493.
35. Jas, G., and Kuczera, K. (2004) Equilibrium structure and folding of a helix-forming peptide: Circular dichroism measurements and replica-exchange molecular dynamics simulations. *Biophys. J.* 87 (6), 3786–3798.
36. Gnanakaran, S., Hochstrasser, R., and Garcia, A. (2004) Nature of structural inhomogeneities on folding a helix and their influence on spectral measurements. *Proc. Natl. Acad. Sci. U.S.A.* 101 (25), 9229–9234.
37. Gnanakaran, S., Hochstrasser, R., and Garcia, A. (2003) Nature of structural inhomogeneities during folding of a helix: Manifestation in IR. *Abstr. Paper Am. Chem. Soc.* 226, U335–U335.
38. Ghosh, T., Garde, S., and Garcia, A. (2003) Role of backbone hydration and salt-bridge formation in stability of alpha-helix in solution. *Biophys. J.* 85 (5), 3187–3193.
39. Armen, R., Alonso, D., and Daggett, V. (2003) The role of alpha-, 3(10)-, and pi-helix in helix → coil transitions. *Protein Sci.* 12 (6), 1145–1157.
40. Vila, J., Ripoll, D., and Scheraga, H. (2001) Influence of lysine content and pH on the stability of alanine-based copolypeptides. *Biopolymers* 58 (3), 235–246.
41. Shirley, W., and Brooks, C. (1997) Curious structure in “canonical” alanine based peptides. *Proteins: Struct., Funct., Genet.* 28 (1), 59–71.
42. Zhang, W., Lei, H. X., Chowdhury, S., and Duan, Y. (2004) F<sub>s</sub>-21 peptides can form both single helix and helix-turn-helix. *J. Phys. Chem. B* 108 (22), 7479–7489.
43. Asher, S., Mikhonin, A., and Bykov, S. (2004) UV Raman demonstrates that alpha-helical polyaniline peptides melt to polyproline II conformations. *J. Am. Chem. Soc.* 126 (27), 8433–8440.
44. Kentsis, A., Mezei, M., Gindin, T., and Osman, R. (2004) Unfolded state of polyaniline is a segmented polyproline II helix. *Proteins: Struct., Funct., Bioinf.* 55 (3), 493–501.
45. Mezei, M., Fleming, P., Srinivasan, R., and Rose, G. (2004) Polyproline II helix is the preferred conformation for unfolded polyaniline in water. *Proteins: Struct., Funct., Genet.* 55 (3), 502–507.
46. Pappu, R., and Rose, G. (2002) A simple model for polyproline II structure in unfolded states of alanine-based peptides. *Protein Sci.* 11 (10), 2437–2455.
47. Shi, Z., Olson, C., Rose, G., Baldwin, R., and Kallenbach, N. (2002) Polyproline II structure in a sequence of seven alanine residues. *Proc. Natl. Acad. Sci. U.S.A.* 99 (14), 9190–9195.
48. Mikhonin, A. V., and Asher, S. A. (2006) Direct UV Raman monitoring of 3(10)-helix and pi-bulge premelting during alpha-helix unfolding. *J. Am. Chem. Soc.* 128 (42), 13789–13795.
49. Mikhonin, A., Asher, S., Bykov, S., and Murza, A. (2007) UV Raman spatially resolved melting dynamics of isotopically labeled polyaniline peptide: Slow alpha-helix melting follows 3(10)-helices and pi-bulges premelting. *J. Phys. Chem. B* 111 (12), 3280–3292.
50. Collins, K. D. (1997) Charge density-dependent strength of hydration and biological structure. *Biophys. J.* 72 (1), 65–76.
51. Collins, K. D. (2004) Ions from the Hofmeister series and osmolytes: Effects on proteins in solution and in the crystallization process. *Methods* 34 (3), 300–311.
52. Collins, K. D., Neilson, G. W., and Enderby, J. E. (2007) Ions in water: Characterizing the forces that control chemical processes and biological structure. *Biophys. Chem.* 128 (2–3), 95–104.
53. Bykov, S., Lednev, I., Ianoul, A., Mikhonin, A., Munro, C., and Asher, S. A. (2005) Steady-state and transient ultraviolet resonance Raman spectrometer for the 193–270 nm spectral region. *Appl. Spectrosc.* 59 (12), 1541–1552.
54. Pettersen, E. F., Goddard, T. D., Huang, C. C., Couch, G. S., Greenblatt, D. M., Meng, E. C., and Ferrin, T. E. (2004) UCSF Chimera—A visualization system for exploratory research and analysis. *J. Comput. Chem.* 25, 1605–1612.
55. Manning, M. C., and Woody, R. W. (1991) Theoretical CD studies of polypeptide helices: Examination of important electronic and geometric factors. *Biopolymers* 31, 569–586.
56. Asher, S. A., Mikhonin, A. V., and Bykov, S. (2004) UV Raman demonstrates that alpha-helical polyaniline peptides melt to polyproline II conformations. *J. Am. Chem. Soc.* 126 (27), 8433–8440.
57. Lednev, I., Karnoup, A., Sparrow, M., and Asher, S. (1999) alpha-helix peptide folding and unfolding activation barriers: A nanosecond UV resonance Raman study. *J. Am. Chem. Soc.* 121 (35), 8074–8086.
58. Wang, Y., Purrello, R., Jordan, T., and Spiro, T. G. (1991) UVRR spectroscopy of the peptide bond. I. Amide S, a nonhelical structure marker, is a CαH bending mode. *J. Am. Chem. Soc.* 113, 6359–6368.
59. Asher, S. A., Ianoul, A., Mix, G., Boyden, M. N., Karnoup, A., Diem, M., and Schweitzer-Stenner, R. (2001) Dihedral psi angle dependence of the amide III vibration: A uniquely sensitive UV resonance Raman secondary structural probe. *J. Am. Chem. Soc.* 123 (47), 11775–11781.
60. Mikhonin, A. V., Bykov, S. V., Myshakina, N. S., and Asher, S. A. (2006) Peptide secondary structure folding reaction coordinate: Correlation between UV Raman amide III frequency, Psi Ramachandran angle, and hydrogen bonding. *J. Phys. Chem. B* 110 (4), 1928–1943.
61. Sharma, B., Bykov, S. V., and Asher, S. A. (2008) UV resonance Raman investigation of electronic transitions in alpha-helical and polyproline II-like conformations. *J. Phys. Chem. B* 112 (37), 11762–11769.
62. Ma, L., Ahmed, Z., Mikhonin, A. V., and Asher, S. A. (2007) UV resonance Raman measurements of poly-L-lysine’s conformational energy landscapes: Dependence on perchlorate concentration and temperature. *J. Phys. Chem. B* 111 (26), 7675–7680.
63. Damodaran, S. (1988) Influence of protein conformation on its adaptability under chaotropic conditions. *Int. J. Biol. Macromol.*, 11.
64. Ma, L., Ahmed, Z., Mikhonin, A., and Asher, S. (2007) UV resonance Raman measurements of poly-L-lysine’s conformational energy landscapes: Dependence on perchlorate concentration and temperature. *J. Phys. Chem. B* 111 (26), 7675–7680.
65. Ramachandran, G. N., and Sasisekharan, V. (1968) Conformation of Polypeptides and Proteins, Vol. 23, pp 283–437, Academic Press, New York.



66. Sundarlingam, M., and Sekharudu, Y. C. (1989) Water-inserted alpha-helical segments implicate reverse turns as folding intermediates. *Science* 244, 1333–1337.
67. Millhauser, G. L. (1995) Views of helical peptides—A proposal for the position of 3(10)-helix along the thermodynamic folding pathway. *Biochemistry* 34 (32), 10318–10318.
68. Beck, D. A. C., White, G. W. N., and Daggett, V. (2007) Exploring the energy landscape of protein folding using replica-exchange and conventional molecular dynamics simulations. *J. Struct. Biol.* 157 (3), 514–523.
69. Hornak, V., Abel, R., Okur, A., Strockbine, B., Roitberg, A., and Simmerling, C. (2006) Comparison of multiple amber force fields and development of improved protein backbone parameters. *Proteins: Struct., Funct., Bioinf.* 65 (3), 712–725.
70. Goto, Y., Takahashi, N., and Fink, A. L. (1990) Mechanism of acid-induced folding of proteins. *Biochemistry* 29, 3480–3488.
71. Thomas, A. S., and Elcock, A. H. (2007) Molecular dynamics simulations of hydrophobic associations in aqueous salt solutions indicate a connection between water hydrogen bonding and the Hofmeister effect. *J. Am. Chem. Soc.* 129 (48), 14887–14898.
72. Collins, K. D., and Washabaugh, M. W. (1985) The Hofmeister effect and the behavior of water at interfaces. *Q. Rev. Biophys.* 18, 323–422.
73. Vila, J. A., Ripoll, D. R., and Scheraga, H. A. (2000) Physical reasons for the unusual alpha-helix stabilization afforded by charged or neutral polar residues in alanine-rich peptides. *Proc. Natl. Acad. Sci. U.S.A.* 97, 13075–13079.
74. Garcia, A. E., and Sanbonmatsu, K. Y. (2002) alpha-helical stabilization by side chain shielding of backbone hydrogen bonds. *Proc. Natl. Acad. Sci. U.S.A.* 99, 2782–2787.
75. Mukherjee, S., Chowdhury, P., and Gai, F. (2006) Tuning the cooperativity of the helix-coil transition by aqueous reverse micelles. *J. Phys. Chem. B* 110, 11615–11619.
76. Debye, P., and Huckel, E. (1923) *Phys. Z.* 24, 185–206.
77. Hol, W. G. J. (1985) The role of the alpha-helix dipole in protein function and structure. *Prog. Biophys. Mol. Biol.* 45, 149–195.
78. Hol, W. G. J., Duijnen, P. T. v., and Berendsen, H. J. C. (1978) The alpha-helix dipole and the properties of proteins. *Nature* 273, 443–446.
79. Shoemaker, K. R., Kim, P. S., York, E. J., Stewart, J. M., and Baldwin, R. L. (1987) Tests of the helix dipole model for stabilization of alpha-helices. *Nature* 326, 573–567.